Paper No.
C2025-00068

AMPP ANNUAL CONFERENCE + EXPO
APRIL 6-10, 2025 | NASHVILLE, TENNESSEE

Effect of SO_2, NO_2, O_2, and Chloride on Duplex and Super Duplex Stainless Steels in CCUS Environments

Xi Wang, Yoon-Seok Choi, Priyanka Adapala,
Maryam Eslami, and Srdjan Nesic
Ohio University
342 W State St.
Athens, OH
USA

Hisashi Amaya, and Kyohei Kanki
Nippon Steel Kansai R&D
1850 Minato
Wakayama City
Japan

ABSTRACT

To significantly reduce CO_2 in the atmosphere, CO_2 must be captured, compressed, and transported to a sequestration site for permanent storage. When injecting CO_2 emitted from various industrial sources into a well, injected fluid and formation water will be in contact with injection strings, which is saturated with CO_2 with corrosive impurities. Corrosion resistant alloys, such as duplex stainless steel and super duplex stainless steel, are candidates for injection tubing. The objective of this work is to evaluate the effect of SO_2, NO_2, O_2, and chloride concentrations on the duplex (S82551) and super duplex (S39274) stainless steels in the aqueous phase under supercritical CO_2 environment. Exposure experiments of samples in 5 or 25 wt% NaCl were carried out at 150°C with 120 bar (1740 psi) CO_2 in a 7L autoclave. Up to 100 ppm of SO_2, NO_2, O_2 were introduced into the autoclave. The steel samples were examined for uniform corrosion and localized corrosion. In supercritical CO_2 environment up to 100 ppm SO_2, both stainless steels showed good corrosion resistance. However, with 100 ppm NO_2, crevice corrosion was observed on the duplex stainless steel. When O_2 was introduced in addition to NO_2, super duplex stainless steel also showed signs of crevice corrosion. The localized attack further intensified with higher chloride concentration. Compared to pitting corrosion and uniform corrosion, crevice corrosion should be emphasized in such an environment.

Keywords: Supercritical CO2; Corrosion resistant alloys; crevice corrosion

INTRODUCTION

Consumption of fossil fuels, such as oil, natural gas, and coal, has increased the concentration of CO_2 in the atmosphere, a known greenhouse gas. To significantly reduce CO_2 emissions from different sources, CO_2 must be captured, compressed, and transported to a sequestration site for permanent storage. When injecting CO_2 emitted from various industrial sources into a well, it is considered that injected fluid and formation water will be in contact with injection strings (tubing, liners, or casings).

Given the corrosivity of formation water saturated with CO_2 at high pressure, plus the presence of contaminants (such as O_2, SO_2, NO_2, etc.), carbon steel appears inadequate for such service. Consequently, corrosion resistant alloys (CRAs) are being considered. Although there are achievements in several carbon capture and storage (CCS) projects and knowledge from research by corrosion tests, the applicability of duplex and super duplex stainless steels is not clear in supercritical CO_2 environment with impurities. Some impurities, e.g. SO_2 and O_2, were studied and showed their potential to be used in aqueous phase in supercritical CO_2 environment[1,2]. However, NO_2 as a common contaminant in the supercritical CO_2 environment has not been studied.

Two 25Cr alloys, super duplex stainless steel (SDSS, UNS S39274) with higher Mo and W contents, and duplex stainless steel (DSS, UNS S82551) with higher Cu content, were selected for this study as they showed superior performance in the previous studies[1,2].

The objective of the study is to evaluate the corrosion behavior of super duplex and duplex stainless steels in chloride solution with supercritical CO_2 and contaminants (O_2, SO_2, and NO_2).

EXPERIMENTAL PROCEDURE

The composition of super duplex stainless steel (S39274) and duplex stainless steel (S82551) are listed in Table 1.

Table 1

Chemical composition of super duplex stainless steel (S39274) and duplex stainless steel (S82551).

UNS#	C	Si	Mn	Cu	Ni	Cr	Mo	W	N	Fe
S39274	≤ 0.03	≤ 0.80	≤ 1.00	0.2~0.8	6.0~8.0	24.0~26.0	2.5~3.5	1.5~2.5	0.24~0.32	Bal.
S82551	≤ 0.03	≤ 0.80	≤ 1.50	2.0~3.0	4.5~6.5	24.5~26.5	0.75~2.0	-	0.10~0.35	Bal.

Two materials were machined into three geometries for weight loss and crevice corrosion evaluation (Figure 1a and b). The exposure specimens were polished to #600 grit, cleaned in deionized water and isopropanol ultrasonic bath, and dried in lab air prior to assembly. Titanium fixtures and polyether ether ketone insulators were used to secure specimens on the shaft. The crevice specimens were assembled as illustrated in Figure 1c forming a metal-to-metal crevice. A torque of 3 N·m was applied to each crevice set.

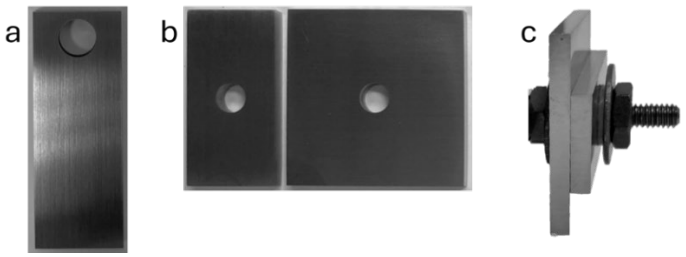

Figure 1: Exposure specimens: a. weight loss specimen (15mm x 40mm x 3mm); b. crevice specimens (15mm x 30mm x 2mm and 30mm x 30mm x 2mm); c. assembled crevice specimens.

Corrosion tests were performed in a high pressure high temperature system, consisting of a 7.5L Hastelloy C276 autoclave, an impurity injection system, and a high pressure CO_2 booster pump. 5L of NaCl solution was prepared and deoxygenated with CO_2 bubbling into the solution before samples were loaded. After sealing the autoclave, the gases was purged on top of the electrolyte in the autoclave. NaCl concentration was 5 wt% for most tests, except that the last test was 25 wt% NaCl. After the autoclave was sealed, impurities were added at room temperature from technical grade SO_2, NO_2, or O_2 cylinders. The required moles of each gas in the autoclave were calculated considering their dissolution in both CO_2 phase and aqueous phase. Then, around 60 bars of CO_2 were added to the autoclave. Subsequently, the autoclave temperature was increased to the testing temperature of 150°C. After the temperature reached 150°C, more CO_2 was added to achieve the total pressure of 125 bar. The total exposure time was 4 days. The test conditions are listed in Table 2.

The solution pH was measured with a ZrO_2-based high temperature high pressure pH electrode at the beginning of the tests after impurities were injected and pressure reached test conditions (125 bar, 150 °C). After tests, samples were collected, rinsed with DI water and isopropanol, and dried with lab air. After each test, corroded surface and corrosion product layers were analyzed using scanning electron microscopy (SEM) and energy dispersive X-ray spectroscopy (EDS). Then, the test specimens were cleaned per ASTM G1[3]. The uniform corrosion rate was calculated based on weight loss. And the localized corrosion rate was defined as the maximum depth of the localized corrosion, measured using optical profilometry on the weight loss and crevice specimens for each condition, divided by exposure time.

$$Uniform\ corrosion\ rate\ (mm/year) = \frac{8.76 \times 10^4 \times weight\ loss\ (g)}{area\ (cm^2) \times density(g/cm^3) \times time(hour)}$$

RESULTS AND DISCUSSION

Six tests were conducted in this study. Table 2 summarizes the test conditions, and results, including both uniform and localized corrosion rates for weight loss and crevice specimens for all tests.

Table 2

Test conditions and corrosion rates. Error bars are max/min range for weight loss (WL) specimens, and standard deviations for crevice specimens.

Test	SO_2 (ppm-mol)	NO_2 (ppm-mol)	O_2 (ppm-mol)	Chloride (wt%)	Measured pH	S39274 Corrosion rate (mm/year)				S82551 Corrosion rate (mm/year)			
						WL specimen		Crevice specimen		WL specimen		Crevice specimen	
						Uniform	Localized	Uniform	Localized	Uniform	Localized	Uniform	Localized
A	100	100	-	5	3.03	<0.01	3.65	0.02 ± 0.03	0.91	<0.01	7.3	0.02 ± 0.03	<0.01
B	100	-	-	5	3.03*	<0.01	-	-	-	<0.01	-	-	-
C	-	100	-	5	2.8	<0.01	7.3	<0.01	1.37	<0.01	11.86	<0.01	5.48
D	-	100	100	5	2.64	0.013 ± 0.004	7.3	0.011 ± 0.005	<0.01	0.010 ± 0.001	<0.01	0.01	3.65
E	-	10	-	5	3.1	0.011 ± 0.005	<0.01	<0.01	<0.01	<0.01	<0.01	<0.01	<0.01
F	-	10	-	25	2.71	0.07 ± 0.02	4.56	0.02 ± 0.01	4.56	0.05 ± 0.01	3.65	0.04 ± 0.02	1.37

*Calculated by OLI Studio

Test A. 100 ppm SO_2 and NO_2

In Test A, 100 ppm SO_2 and 100 ppm NO_2 were introduced in the autoclave. According to the acid formation reaction between NO_2 and SO_2 in water[4],

$$SO_2 + NO_2 + H_2O \rightarrow NO + H_2SO_4, \quad (1)$$

the solution pH will be lower than the pure CO_2 environment, which could be a threat to the passive film stability to stainless steels. The solution pH was measured around 3 in Test A (Table 2), but both SDSS and DSS showed very low uniform corrosion rate, which means that the passive films of both CRAs are still protective at this pH. However, the insulating washer area (squared in Figure 2) of SDSS and DSS showed crevice attack over 30 μm of depth. Therefore, crevice specimens were added to examine the severity of crevice corrosion (Figure 3).

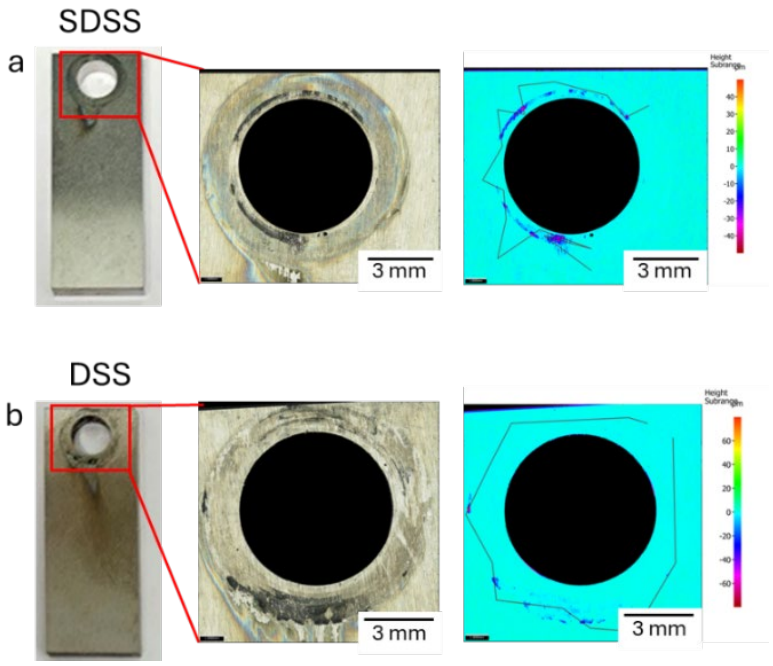

Figure 2: As-cleaned weight loss specimens of Test A 100 ppm SO_2 and 100 ppm NO_2. a. Optical images and optical profilometry of SDSS; b. Optical images and optical profilometry of DSS.

Figure 3 and Figure 4 are the results of crevice specimens in Test A with 100 ppm SO_2 and 100 ppm NO_2. Both SDSS and DSS crevice specimens in Test A showed discoloration inside crevices (Figure 3a and Figure 4a). However, SDSS crevice specimens had some crevice attack around 10 μm as illustrated in Figure 3b, while DSS did not have notable depth change across the crevice (Figure 4b). According to SEM/EDS (Figure 3c) of SDSS, the corrosion product inside crevice was rich in Cr, Mo, W, and O, and depleted in Fe. Though the crevice corrosion attack was not severe on DSS, a thin layer of corrosion product was present with O detected inside the crevice as shown in Figure 4c, where the polishing lines were still visible.

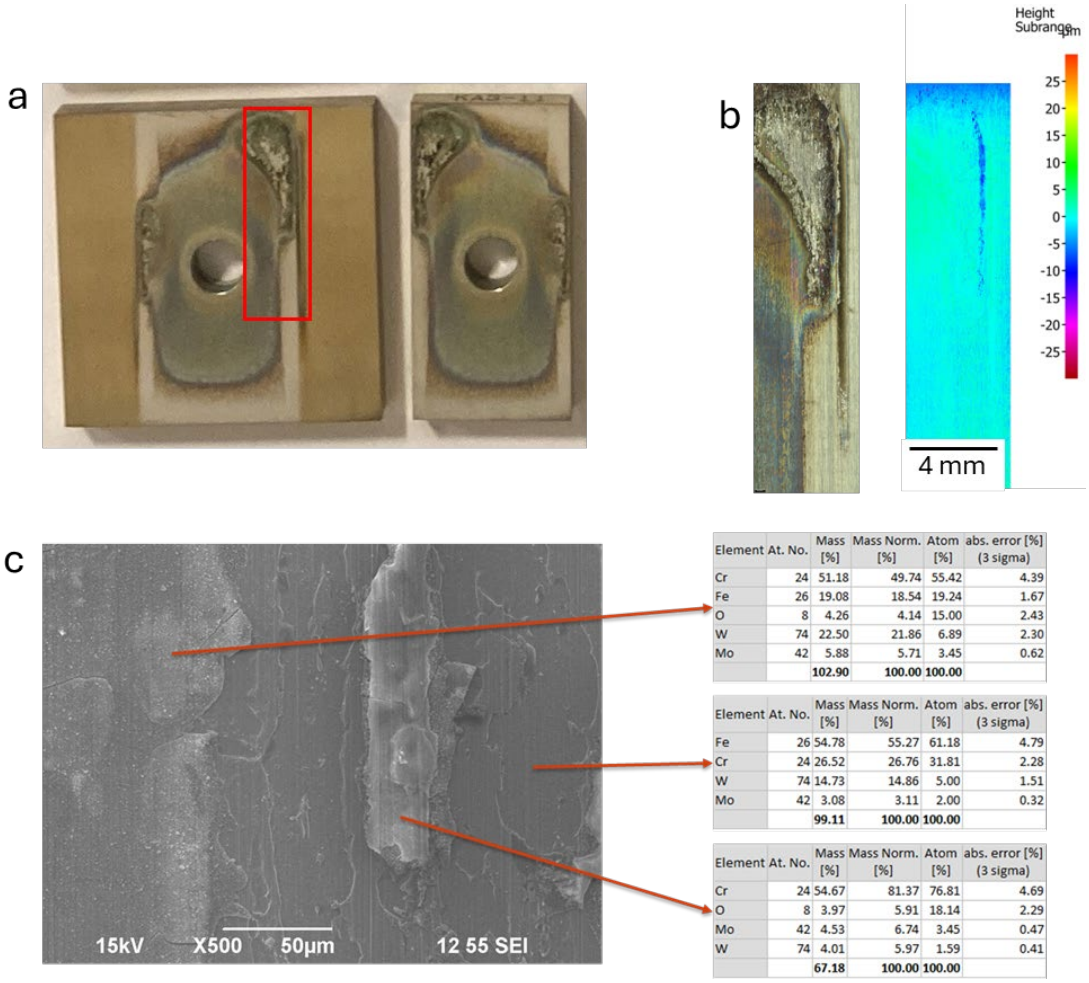

Element	At. No.	Mass [%]	Mass Norm. [%]	Atom [%]	abs. error [%] (3 sigma)
Cr	24	51.18	49.74	55.42	4.39
Fe	26	19.08	18.54	19.24	1.67
O	8	4.26	4.14	15.00	2.43
W	74	22.50	21.86	6.89	2.30
Mo	42	5.88	5.71	3.45	0.62
		102.90	**100.00**	**100.00**	

Element	At. No.	Mass [%]	Mass Norm. [%]	Atom [%]	abs. error [%] (3 sigma)
Fe	26	54.78	55.27	61.18	4.79
Cr	24	26.52	26.76	31.81	2.28
W	74	14.73	14.86	5.00	1.51
Mo	42	3.08	3.11	2.00	0.32
		99.11	**100.00**	**100.00**	

Element	At. No.	Mass [%]	Mass Norm. [%]	Atom [%]	abs. error [%] (3 sigma)
Cr	24	54.67	81.37	76.81	4.69
O	8	3.97	5.91	18.14	2.29
Mo	42	4.53	6.74	3.45	0.47
W	74	4.01	5.97	1.59	0.41
		67.18	**100.00**	**100.00**	

Figure 3: Test A (100 ppm SO_2 + 100 ppm NO_2) SDSS crevice results. a. As-exposed SDSS crevice specimens; b. Optical image and profilometry of highlighted area in a on the as-cleaned SDSS crevice specimen; c. SEM and elemental analysis of crevice area.

Both alloys did not suffer from pitting corrosion, which indicates that the passive layers were stable for both DSS and SDSS in the environment. However, once crevice corrosion initiates, metal ion hydrolysis occurs, leading to a further decrease in the crevice pH. This acidification drives the migration of chloride ions into the crevice, exacerbating the corrosive environment. As a result, the substrate begins to actively corrode within the crevice.

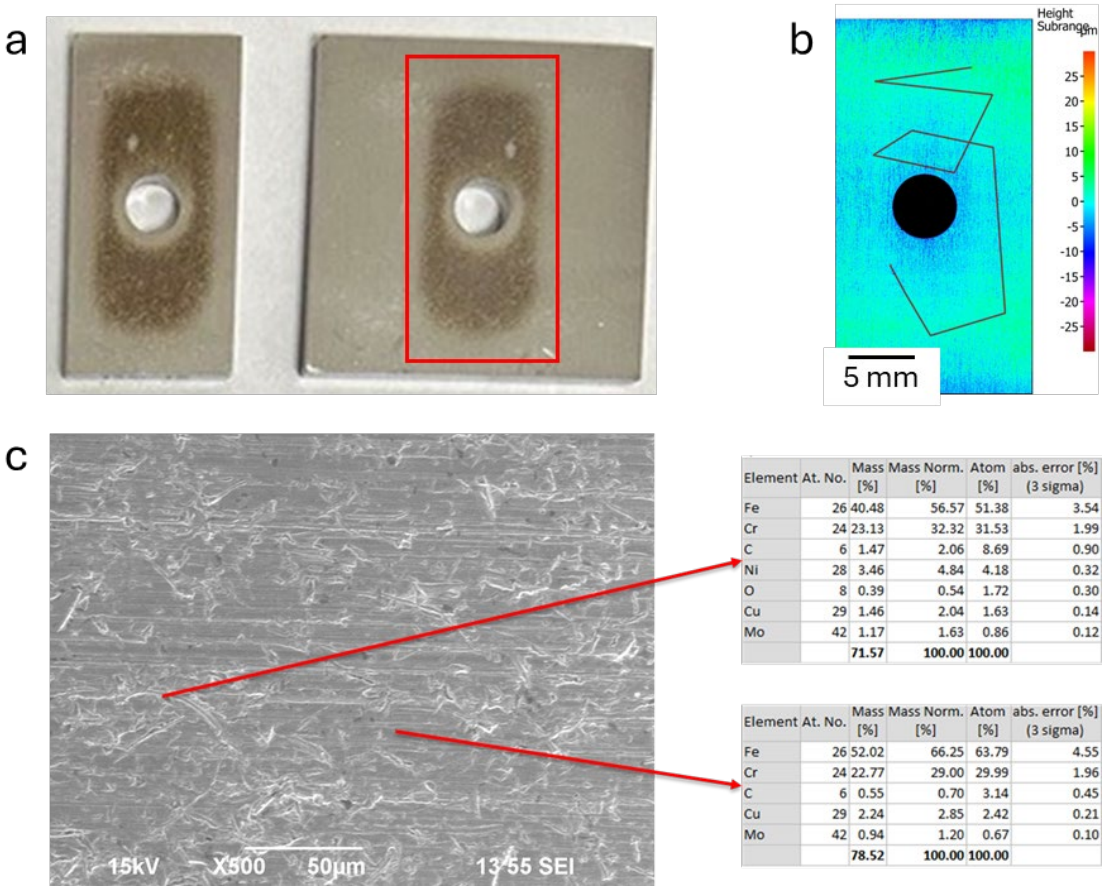

Element	At. No.	Mass [%]	Mass Norm. [%]	Atom [%]	abs. error [%] (3 sigma)
Fe	26	40.48	56.57	51.38	3.54
Cr	24	23.13	32.32	31.53	1.99
C	6	1.47	2.06	8.69	0.90
Ni	28	3.46	4.84	4.18	0.32
O	8	0.39	0.54	1.72	0.30
Cu	29	1.46	2.04	1.63	0.14
Mo	42	1.17	1.63	0.86	0.12
		71.57	**100.00**	**100.00**	

Element	At. No.	Mass [%]	Mass Norm. [%]	Atom [%]	abs. error [%] (3 sigma)
Fe	26	52.02	66.25	63.79	4.55
Cr	24	22.77	29.00	29.99	1.96
C	6	0.55	0.70	3.14	0.45
Cu	29	2.24	2.85	2.42	0.21
Mo	42	0.94	1.20	0.67	0.10
		78.52	**100.00**	**100.00**	

Figure 4: Test A (100 ppm SO_2 + 100 ppm NO_2) DSS crevice results. a. As-exposed DSS crevice specimens; b. Optical image and profilometry of highlighted area in a on the as-cleaned DSS crevice specimen; c. SEM and elemental analysis of crevice area.

Test B. 100 ppm SO_2

To further understand the effect of SO_2 and NO_2, they were evaluated separately (Test B and C in Table 2). According to Test B (Figure 5), the exposure specimens did not show any sign of either uniform corrosion or localized attacks. Only some sub-micron pits were observed with SEM (Figure 5c and g). Therefore, 100 ppm SO_2 alone could not induce localized threat, which aligns with a previous study[2].

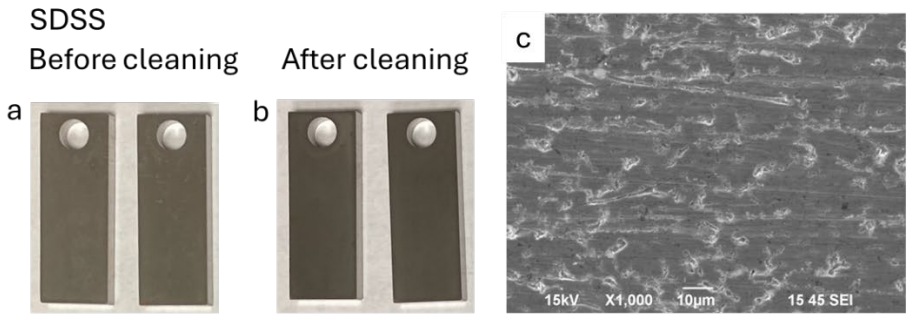

d

Element	At. No.	Mass [%]	Mass Norm. [%]	Atom [%]	abs. error [%] (3 sigma)
C	6	0.64	0.83	3.58	0.53
O	8	0.38	0.49	1.59	0.34
Si	14	0.81	1.05	1.95	0.25
S	16	1.28	1.65	2.68	0.20
Cr	24	22.23	28.76	28.78	2.04
Fe	26	46.41	60.05	55.95	4.25
Ni	28	4.40	5.70	5.05	0.70
W	74	1.14	1.47	0.42	1.21
		77.29	**100.00**	**100.00**	

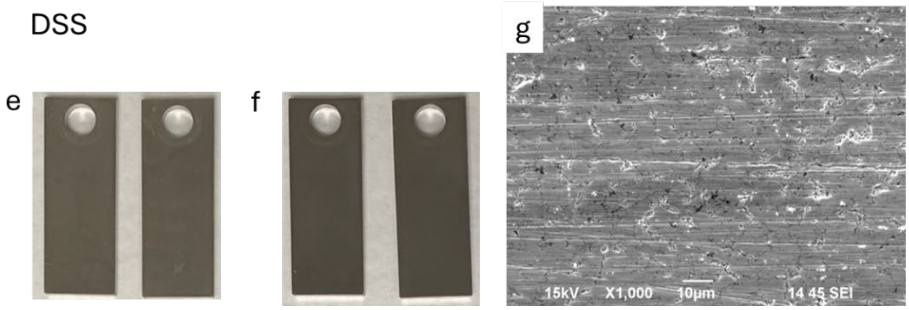

h

Element	At. No.	Mass [%]	Mass Norm. [%]	Atom [%]	abs. error [%] (3 sigma)
C	6	0.55	0.64	2.85	0.48
Si	14	1.10	1.29	2.46	0.22
Cr	24	24.23	28.39	29.16	2.22
Fe	26	51.41	60.24	57.60	4.70
Ni	28	4.58	5.37	4.89	0.73
Cu	29	2.32	2.72	2.29	0.64
Mo	42	1.15	1.35	0.75	0.28
		85.35	**100.00**	**100.00**	

Figure 5: Test B (100 ppm SO_2) results: photos of a. as-exposed and b. as-cleaned SDSS weight loss specimens; c. SEM image of a; d. EDS of c; and photos of e. as-exposed and f. as-cleaned DSS weight loss specimens; g. SEM image of e; EDS of h.

Test C. 100 ppm NO_2

However, in Test C with 100 ppm NO_2, the weight loss specimens of both materials showed a few severe crevice attacks around the insulating washers as deep as 100 μm. Therefore, crevice samples were evaluated as shown in Figure 6 and Figure 7. Both samples had corrosion attack inside the crevice. DSS (Figure 7b) had one spot inside crevice measured around 45 μm deep, while the crevice attack on SDSS was around 10 μm. The edge of SDSS crevice was etched left grain shape corrosion marks, which looked like selective dissolution[5], and EDS showed the area was rich in Fe, Cr, Mo, and Si. According to EDS, inside of the SDSS crevice, thick corrosion products accumulated, rich in Fe, Cr, Mo, and O.

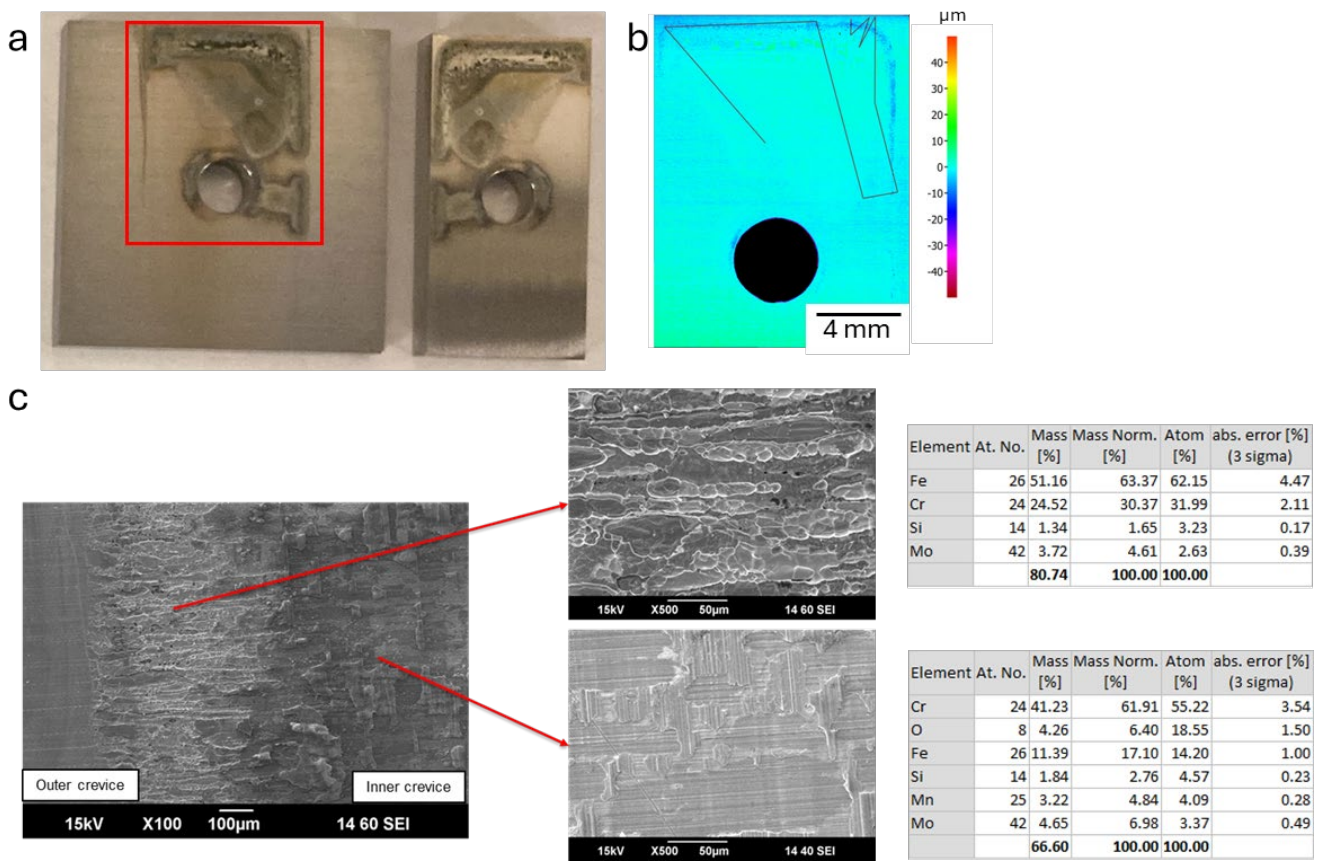

Element	At. No.	Mass [%]	Mass Norm. [%]	Atom [%]	abs. error [%] (3 sigma)
Fe	26	51.16	63.37	62.15	4.47
Cr	24	24.52	30.37	31.99	2.11
Si	14	1.34	1.65	3.23	0.17
Mo	42	3.72	4.61	2.63	0.39
		80.74	**100.00**	**100.00**	

Element	At. No.	Mass [%]	Mass Norm. [%]	Atom [%]	abs. error [%] (3 sigma)
Cr	24	41.23	61.91	55.22	3.54
O	8	4.26	6.40	18.55	1.50
Fe	26	11.39	17.10	14.20	1.00
Si	14	1.84	2.76	4.57	0.23
Mn	25	3.22	4.84	4.09	0.28
Mo	42	4.65	6.98	3.37	0.49
		66.60	**100.00**	**100.00**	

Figure 6: Test C (100 ppm NO_2) SDSS crevice results. a. Photo of as-exposed SDSS crevice specimens; b. optical profilometry of selected area in a after cleaning; c. SEM images and elemental analysis of SDSS crevice area.

The edge of DSS crevice was covered by sponge like corrosion products, rich in Cr, Cu, Ni and O. Inside the DSS crevice, the thicker corrosion product layer was rich in Cr, Mo-oxides, and the thinner corrosion product layer was rich in Cr, Fe, Mo, and O. Therefore, the addition of NO_2 likely induces crevice corrosion.

NO_2 is highly soluble in water and reacts with water to produce nitric acid and nitric oxide[6]:

$$3NO_2 + H_2O \rightleftharpoons 2HNO_3 + NO \quad (2)$$

The formation of HNO_3 can be confirmed by the measured pH of 2.8 in Test C (Table 2). HNO_3 corrosion is known to be a complex process due to the autocatalytic nature of NO_3^- reduction, which is the primary cathodic reaction[7].

$$NO_3^- + 3H^+ + 2e^- \rightleftharpoons HNO_2 + H_2O \quad (3)$$

The redox potential of this reaction is higher than hydrogen evolution reaction, which increases the corrosion potential of stainless steel. It can be speculated that the potential drop along the crevice due to the combination of crevice geometry, and the additional HNO_3 cathodic reaction outside crevice could induce crevice corrosion. However, the effect of nitric acid on crevice corrosion has not been broadly studied.

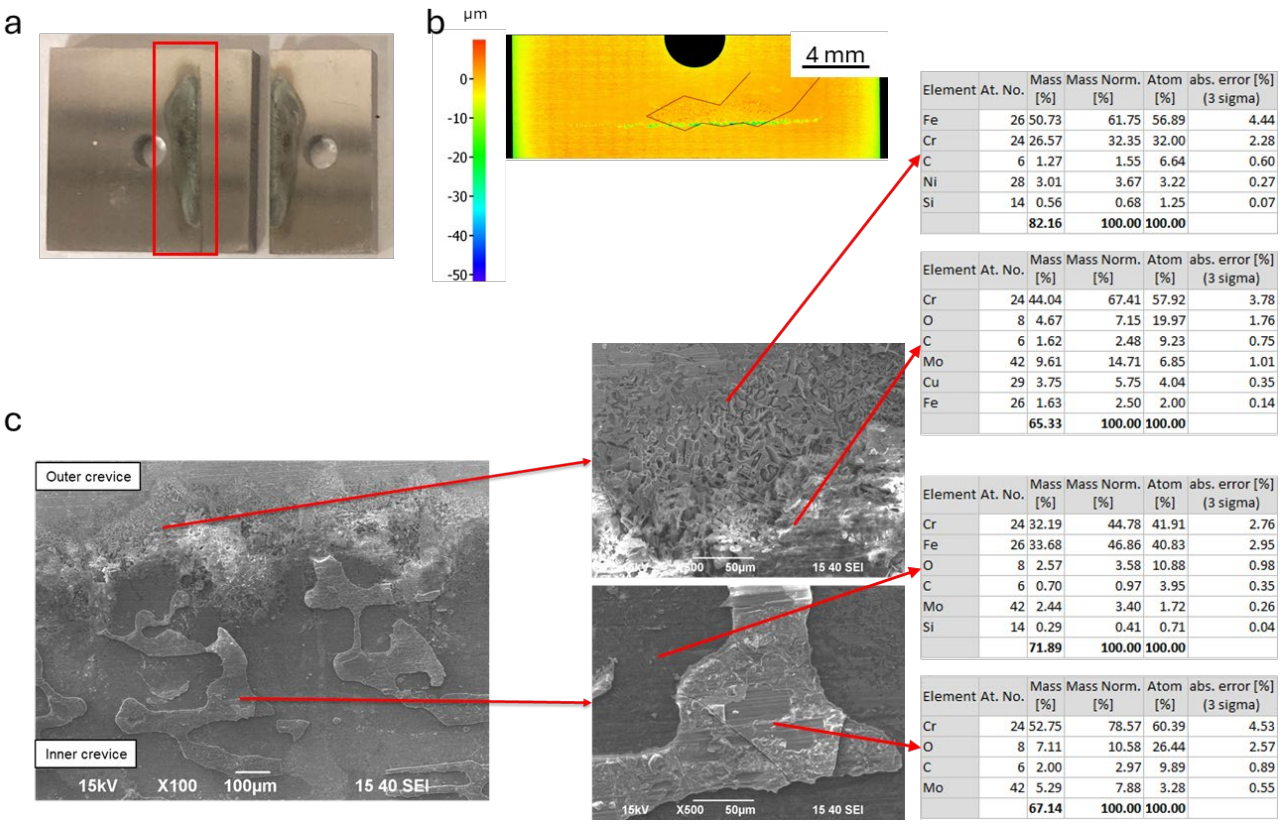

Element	At. No.	Mass [%]	Mass Norm. [%]	Atom [%]	abs. error [%] (3 sigma)
Fe	26	50.73	61.75	56.89	4.44
Cr	24	26.57	32.35	32.00	2.28
C	6	1.27	1.55	6.64	0.60
Ni	28	3.01	3.67	3.22	0.27
Si	14	0.56	0.68	1.25	0.07
		82.16	**100.00**	**100.00**	

Element	At. No.	Mass [%]	Mass Norm. [%]	Atom [%]	abs. error [%] (3 sigma)
Cr	24	44.04	67.41	57.92	3.78
O	8	4.67	7.15	19.97	1.76
C	6	1.62	2.48	9.23	0.75
Mo	42	9.61	14.71	6.85	1.01
Cu	29	3.75	5.75	4.04	0.35
Fe	26	1.63	2.50	2.00	0.14
		65.33	**100.00**	**100.00**	

Element	At. No.	Mass [%]	Mass Norm. [%]	Atom [%]	abs. error [%] (3 sigma)
Cr	24	32.19	44.78	41.91	2.76
Fe	26	33.68	46.86	40.83	2.95
O	8	2.57	3.58	10.88	0.98
C	6	0.70	0.97	3.95	0.35
Mo	42	2.44	3.40	1.72	0.26
Si	14	0.29	0.41	0.71	0.04
		71.89	**100.00**	**100.00**	

Element	At. No.	Mass [%]	Mass Norm. [%]	Atom [%]	abs. error [%] (3 sigma)
Cr	24	52.75	78.57	60.39	4.53
O	8	7.11	10.58	26.44	2.57
C	6	2.00	2.97	9.89	0.89
Mo	42	5.29	7.88	3.28	0.55
		67.14	**100.00**	**100.00**	

Figure 7: Test C (100 ppm NO_2) DSS crevice results. a. Photo of as-exposed DSS crevice specimens; b. optical profilometry of selected area in a after cleaning; c. SEM images and elemental analysis of SDSS crevice area.

Test D. 100 ppm NO_2 and O_2

It is known that higher concentration of dissolved oxygen leads to higher cathodic limiting current, and thus increases the corrosion potential above the pitting potential, where pitting corrosion could occur. In a previous study, SDSS and DSS did not show pitting susceptibility up to 5000 ppm O_2 in 5 wt% NaCl at 100°C under supercritical CO_2, but crevice corrosion occurred with high concentration of dissolved oxygen[1]. Therefore, in Test D, 100 ppm O_2 was introduced in addition to 100 ppm NO_2 to evaluate the effect of O_2 in the presence of NO_2. Figure 5 illustrates the results of Test D (100 ppm NO_2 + 100 ppm O_2). SDSS had crevice corrosion (Figure 8a-d) with deepest attack around 10 µm similar to Test C (Figure 7a-c). However, DSS suffered pitting corrosion in addition to crevice corrosion, and the deepest pit was around 25 µm (Figure 8f).

The pH decreased to 2.64 in the presence of NO_2 and O_2 in Test D due to the regeneration of NO_2 from NO and O_2[6],

$$2NO + O_2 \rightleftharpoons 2NO_2 \qquad (4)$$

and further formation of HNO_3. The above series reactions led to the pitting corrosion on DSS where its passivity was challenged due to lower solution pH.

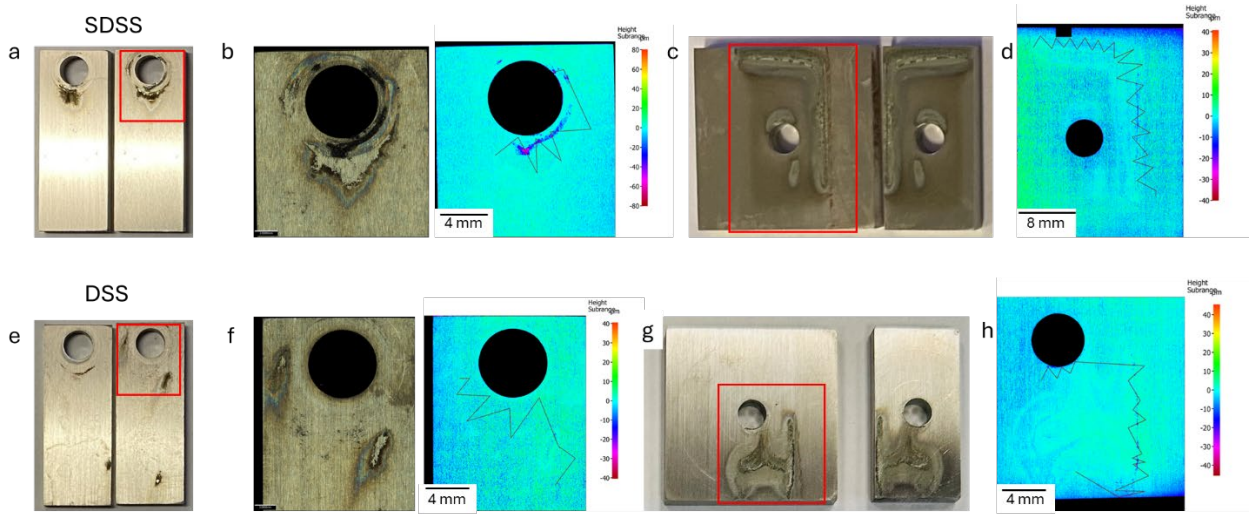

Figure 8: Test D (100 ppm NO_2 + 100 ppm O_2) results. a. As-exposed SDSS weight loss samples; b. optical image and profilometry of as-cleaned SDSS specimens; c. as exposed SDSS crevice specimens; d. optical profilometry of area in c after cleaning. e. As-exposed DSS weight loss samples; f. optical image and profilometry of as-cleaned DSS specimens; g. as exposed SDSS crevice specimens; h. optical profilometry of area in c after cleaning.

Test E. 10 ppm NO_2

In order to understand if less NO_2 will still induce crevice corrosion, only 10 ppm NO_2 was added to the system. Corrosion was not observed upon visual inspection (Figure 9a, b, d, e). There was only slight etch inside the crevice region on SDSS (Figure 9c) where polishing marks was still visible, but a thin layer of corrosion products was on top of the substrate. In Test E, uniform corrosion rate was low for both alloys, and localized attack was not found.

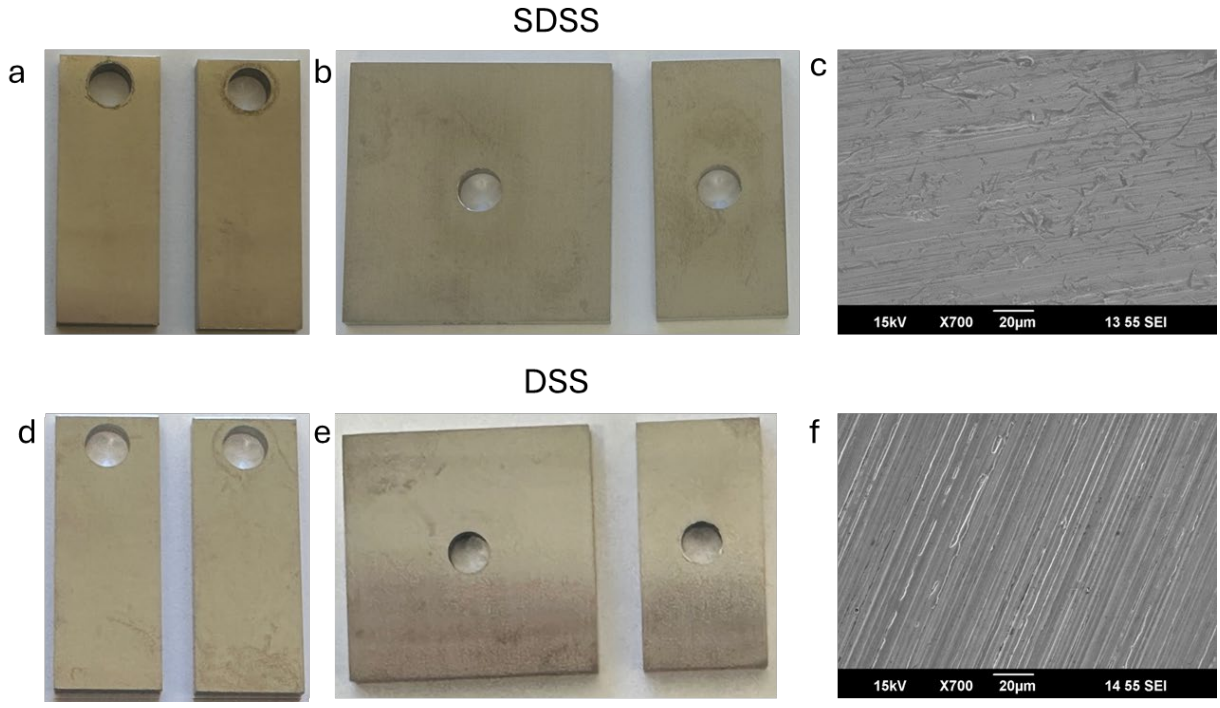

Figure 9: Photos of Test E (10 ppm NO_2 and 5 wt% NaCl): a. SDSS weight loss specimens; b. SDSS crevice specimens; c. SEM image of inner crevice area on a SDSS crevice specimen; d. DSS

weight loss specimens; e. DSS crevice specimens; f. SEM image of inner crevice area on DSS a crevice specimen.

Test F. 10 ppm NO_2 and 25 wt% NaCl

Another important factor that can affect the SDSS and DSS corrosion performance is chloride concentration, so 25 wt% NaCl was added to the system to evaluate the effect of chloride concentration. As shown in Figure 10, strong discoloration was observed on both SDSS weight loss and crevice specimens (Figure 10a and e). After cleaning, the washer area was dark, so optical profilometry was conducted in that area. Localized attack as deep as 40 µm was captured as illustrated in Figure 10d. The entire crevice area seemed to be etched with a few darker spots on the crevice specimens (Figure 10f). The deepest spot was about 40 µm in depth.

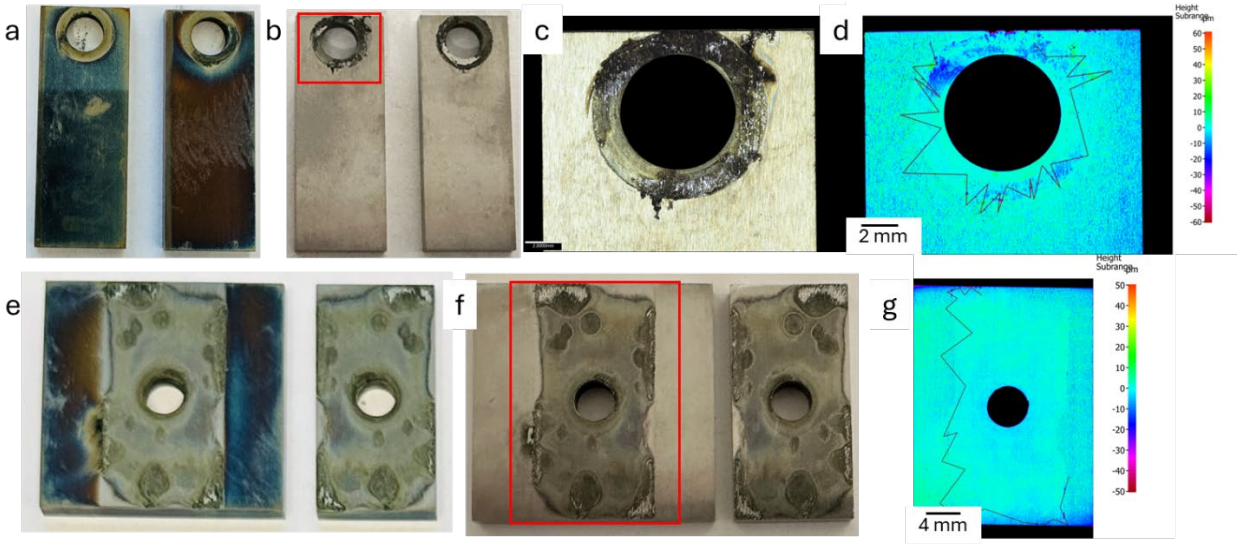

Figure 10: Test F (10 ppm NO_2 + 25 wt% NaCl), SDSS results: a. photo of as-exposed SDSS weight loss specimens; b. photo of as-cleaned SDSS weight loss specimens; c. optical image of selected area in b; d. surface profile of c; e. photo of as-exposed SDSS crevice specimens; f. photo of as-cleaned SDSS crevice specimens; g. surface profile of selected area in f.

Like SDSS, DSS also showed strong discoloration on all samples, though its corrosion around the washer was more extensive (Figure 11c) but shallower (Figure 11d) than SDSS (Figure 10c and d). However, pits were found on DSS weight loss specimens in addition to abovementioned crevice corrosion as shown in Figure 11b. In addition, the discoloration inside the crevice after exposure (Figure 11e and f) seemed more severe than SDSS (Figure 10e and f), but the attack was slightly shallower (Figure 11g).

Abundant chloride can decrease pH of solution saturated by CO_2, which is called salting out effect[8–10]. In the supercritical CO_2 environment, the pH is as low as 3.1 (Test E) without high level of impurities. High salinity could push solution pH to a lower level where both uniform corrosion and localized corrosion were enhanced like Test E. In addition, the abundant chloride itself can be responsible for higher localized corrosion, since high chloride could breakdown the passive film and causes localized attack initiation[11].

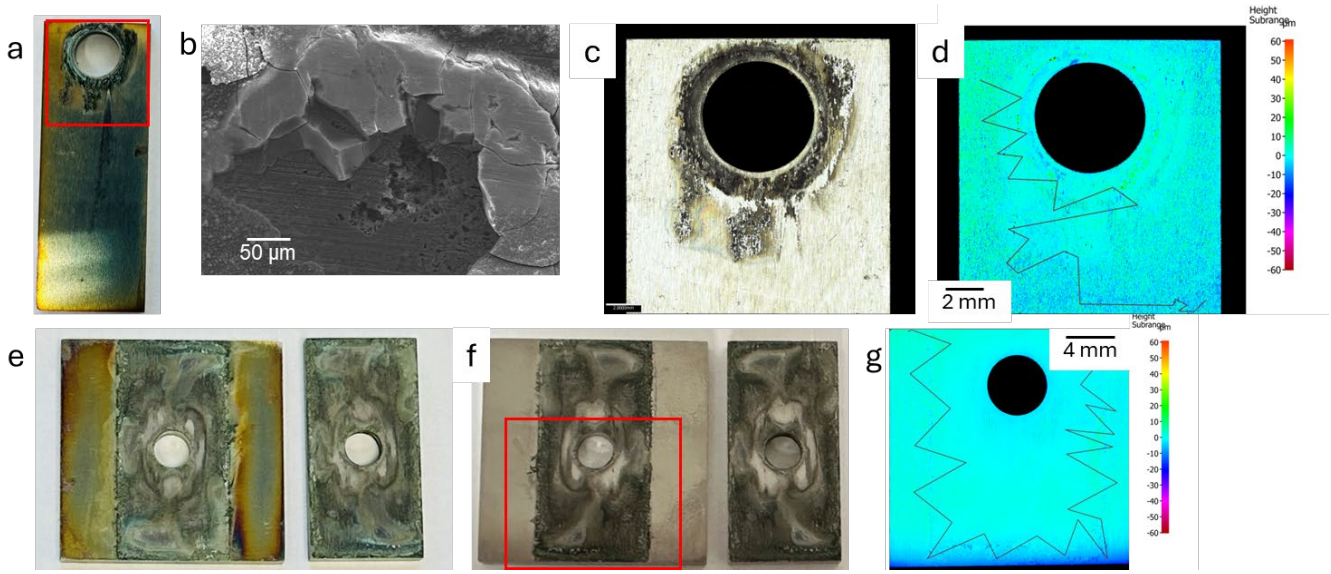

Figure 11: Test F (10 ppm NO_2 + 25 wt% NaCl), DSS results: a. photo of as-exposed DSS weight loss specimens; b. photo of as-cleaned DSS weight loss specimens; c. optical image of selected area in b; d. surface profile of c; e. photo of as-exposed DSS crevice specimens; f. photo of as-cleaned SDSS crevice specimens; g. surface profile of selected area in f.

CONCLUSIONS

The study was set out to understand the effects of NO_2, SO_2, O_2, and chloride concentrations on corrosion behavior of super duplex stainless steel and duplex stainless steel in aqueous phase in supercritical CO_2 environment at 150 °C. Following conclusions can be drawn from this study:

- Super duplex stainless steel and duplex stainless steel showed a passive behavior at test conditions with overall corrosion rates less than 0.1 mm/year.
- The addition of SO_2 did not increase the localized corrosion susceptibility for both alloys.
- The addition of NO_2 could induce crevice corrosion for both alloys, but the underlying mechanism is not well understood.
- The addition of O_2 in the presence of NO_2 could enhance crevice corrosion for both alloys, even increase the pitting susceptibility for duplex stainless steel.
- The addition of SO_2 in the presence of NO_2 could reduce crevice corrosion for both alloys, because the amount of oxidant (HNO_3) is thought to have been reduced by the chemical reaction of H_2SO_4 formation.
- High salinity could reduce solution pH and localized corrosion susceptibility increases.

REFERENCES

1. Kanki, K., Arai, Y., Matsuo, D. & Amaya, H., "Corrosion Resistance of Duplex Stainless Steels for CCS Application under the Liquid Phase in Equilibrium with Supercritical CO_2 Containing Slight Amount of O_2," *AMPP Annual Conference + Expo 2024* Paper No. C2024-20598 (New Orleans, LA: AMPP, 2024).

2. Matsuo, D., Sagara, M., Arai, Y., Amaya, H. & Kanki, K., "Corrosion Resistance of Super Duplex Stainless Steel for CCS Usage under Supercritical CO_2 Conditions with Impurity Gas," *AMPP Annual Conference + Expo 2022* Paper No. 17602 (San Antonio, TX: AMPP, 2022).

3. ASTM[(1)] G1-03. "Standard Practice for Preparing, Cleaning, and Evaluating Corrosion Test Specimens" (West Conshohocken, PA: ASTM).

4. Morland, B. H., Dugstad, A. & Svenningsen, G., "Experimental based CO_2 transport specification ensuring material integrity". *Int. J. Greenh. Gas Control* **119** (2022), 1–10.

5. Aoki, S. & Engelberg, D. L., "Time-Lapse Observation of Crevice Corrosion in Grade 2205 Duplex Stainless Steel". *Materials* **16** (2023), 1–13.

6. Halseid, M., Dugstad, A. & Morland, B., "Corrosion and bulk phase reactions in CO_2 transport pipelines with impurities: Review of recent published studies". *Energy Procedia* **63** (2014), 2557–2569.

7. Shams el Din, A. M. & Fakhr, M. Y., "A thermometric study of the reaction between Fe and HNO_3". *Corros. Sci.* **14** (1974), 635–644.

8. Gao, X. *et al.,* "A Quantitative Study of $FeCO_3$ Solubility in Non-ideal Solutions". NACE CORROSION 2021 Paper No. 16964 (Virtual: NACE, 2021)

9. Madani Sani, F., Brown, B. & Nesic, S., "An Electrochemical Study of the Effect of High Salt Concentration on Uniform Corrosion of Carbon Steel in Aqueous CO_2 Solutions". *J. Electrochem. Soc.* **168** (2023), 051501.

10. Ma, Z., Gao, X., Brown, B., Nesic, S. & Singer, M., "Improvement to Water Speciation and FeCO3Precipitation Kinetics in CO_2 Environments: Updates in NaCl Concentrated Solutions". *Ind. Eng. Chem. Res.* **60** (2021), 17026–17035.

11. Pardo, A. *et al.*, “Influence of pH and Chloride Concentration on the Pitting and Crevice Corrosion Behavior of High-Alloy Stainless Steels”. *Corrosion* **56** (2000), 411–418.

[(1)] ASTM International, 100 Barr Harbor Dr., West Conshohocken, PA 19428-2959.